Observations from Cyclic Tests on Deep, Wide-Flange Beam-Columns

GULEN OZKULA, JOHN HARRIS and CHIA-MING UANG

ABSTRACT

As part of a National Institute of Standards and Technology (NIST) comprehensive research program to study the seismic behavior and design of deep, wide-flange structural steel beam-column members for application in seismic design and construction of steel special moment frames, 25 deep column specimens were subjected to inelastic cyclic loading with three different levels of constant compression axial load (C_a = 0.2, 0.4 and 0.6). The test matrix included five W24 sections (W24×55 to W24×176) to cover a wide range of element slenderness ratios for flange and web local buckling and member slenderness ratios for lateral-torsional buckling and weak-axis flexural buckling. The specimens satisfied AISC 341 requirements for highly or moderately ductile elements. All specimens were subjected to strong-axis bending, except for three specimens that were subjected to weak-axis bending and one specimen that was subjected to biaxial bending. Test results showed that the slenderness ratios had a significant effect on the failure mode—local versus global buckling. The presence of an axial load produced significant local buckling and axial shortening. The level of axial load also affected the plastic rotation capacity. Specimens with weak-axis bending were ductile, showing no local buckling up to a high story-drift ratio. Most of the strong-axis bending specimens were not able to deliver a plastic rotation of 0.03 radians.

Keywords: Beam-column, cyclic behavior, plastic rotation, local buckling, lateral-torsional buckling.

INTRODUCTION

Research on the cyclic behavior of W14 columns under high axial load and seismic drift for braced frame applications has been conducted by Newell and Uang (2008). For special moment frame (SMF) design, however, designers prefer to use deeper columns (e.g., W24 to W36 sections) to satisfy code-enforced story-drift limits. Because the cross-section element and member slenderness ratios are significantly high for deep columns, this class of columns is prone to various forms of local and global buckling that may impair their lateral drift capacity and gravity load-carrying strength. Unfortunately, minimal experimental research is available to support the seismic design or assessment provisions in AISC 341 (AISC, 2010a) and ASCE 41 (ASCE, 2013) for these deeper columns. To fill this gap, NIST developed a comprehensive research plan to study the seismic behavior and design of the wide-flange structural steel beam-column members (NIST, 2011). The plan included studies at the member, subassemblage and system levels. The first step in implementing this plan was to experimentally evaluate the cyclic behavior of plastic hinges in deep columns. Test results will then be used by NIST to validate computational models and to improve seismic design provisions for these types of columns. This paper presents observations from this test series. A detailed report of the testing program and data will be released in the future. Evaluation of the test data and their impact on seismic design and assessment provisions is ongoing.

TEST SETUP AND SPECIMENS

Twenty-five W24 specimens were subjected to three different levels of constant axial load combined with cyclic story-drift demands; see Table 1 for the test matrix—only 21 of the 25 tests are presented in this paper. Five wide-flange sections were selected in order to cover a wide range of element slenderness ratios for flange local buckling (FLB) and web local buckling (WLB). The use of lighter sections (W24×84 and W24×55) also widened the range of member slenderness ratios for lateral-torsional buckling (LTB) and weak-axis flange buckling (FB). Figure 1 shows a comparison of the flange and web width-to-thickness ratios to the seismically compact limits prescribed in AISC 341. The limiting width-to-thickness ratios for highly ductile (λ_{hd}) and moderately ductile (λ_{md}) elements are also shown in Figure 1. For FLB,

Gulen Ozkula, Graduate Student Researcher, University of California, San Diego, CA. Email: gozkula@ucsd.edu

John Harris, Research Structural Engineer, National Institute of Standards and Technology, Washington, DC. Email: john.harris@nist.gov

Chia-Ming Uang, Professor, University of California, San Diego, CA. Email: cmu@ucsd.edu (corresponding)

Paper No. 2015-16

Table 1. Test Matrix

Group No.	Shape	Specimen Designation	Normalized Slenderness $\frac{b_f/2t_r}{\lambda_{hd}}$	Normalized Slenderness $\frac{h/t_w}{\lambda_{hd}}$	Normalized Slenderness $\frac{L}{L_{hd}}$	Normalized Slenderness $\frac{L}{r_y}$	Column Axial Load C_a	Column Axial Load P (kips)	Bending Direction
1	W24×176	1L 1M 1H	0.67	0.57 0.61 0.66	1.42	71.1	0.2 0.4 0.6	465 931 1396	Strong axis
2	W24×131	2Z 2L 2L-P 2M 2H	0.93	0.66 0.70 0.70 0.76 0.82	1.46	72.7	0.0 0.2 0.2 0.4 0.6	0 347 347 693 1040	
3	W24×104	3L 3M 3H	1.18	0.85 0.91 1.00	1.49	74.2	0.2 0.4 0.6	276 551 826	
4	W24×84	4L 4M	0.81	0.91 0.98	2.22	110.8	0.2 0.4	222 445	
5	W24×55	5L 5LM 5M	0.81	1.08 1.12 1.26	3.23	161.2	0.2 0.3 0.4	146 219 292	
6	W24×131	6L 6L-P 6H	0.93	0.70 0.70 0.82	1.46	72.7	0.2 0.2 0.6	347 347 1040	Weak axis
7	W24×131	7M	0.93	0.76	1.46	72.7	0.4	693	Biaxial axis
8	W24×131	8M	0.93	0.76	1.46	72.7	0.4	693	Strong axis, Near-fault

$$\lambda_{hd} = 0.3\sqrt{E/F_y} \quad (1a)$$

$$\lambda_{hd} = 0.38\sqrt{E/F_y} \quad (1b)$$

and for WLB when $C_a = P/\phi_c P_y$ is larger than 0.125,

$$\lambda_{hd} = 0.77\sqrt{E/F_y}\,(2.93 - C_a) \geq 1.49\sqrt{E/F_y} \quad (2a)$$

$$\lambda_{hd} = 1.12\sqrt{E/F_y}\,(2.33 - C_a) \geq 1.49\sqrt{E/F_y} \quad (2b)$$

In Table 1, the unbraced length, L, is also normalized by L_{hd} and $r_{y,}$ respectively, where

$$L_{hd} = 0.086 r_y E/F_y \quad (3)$$

Note that L_{hd} is the limiting unbraced length for beams, but not columns, for a SMF in AISC 341. Specimens were designated "L," "M" and "H" to represent low (C_a = 0.2), medium (C_a = 0.4), and high (C_a = 0.6) axial load levels, respectively. Only one specimen (2Z) was tested without any axial load. Pseudo-static cyclic lateral displacement used for testing followed that specified in Section K2.4b of AISC 341 (2010a) for the majority of column specimens. Two specimens (2L-P and 6L-P) were tested monotonically, one for strong-axis and the other one for weak-axis bending. Specimen 7M was tested with biaxial bending, and specimen 8M was tested by using a near-field loading protocol. Each specimen was 18 ft long with 3-in.-thick base plates welded at each end. ASTM A992 (ASTM, 2012) steel was specified for the column specimens. The material properties obtained from tensile coupon tests are summarized in Table 2.

The overall view of the test setup is shown in Figure 2. Testing was conducted in the Seismic Response Modification Device (SRMD) Test Facility at the University of California, San Diego. As shown in Figure 2, beam-column specimens were tested in a horizontal position with one end attached to a strong wall fixture, while the other end was attached to a reaction block on the shake table. Both ends of the column specimens were welded to the end plates with complete-joint-penetration (CJP) welds. All specimens were tested with presumed fixed-fixed boundary conditions; lateral drift data presented in this paper have been adjusted for rotational flexibility in the boundary conditions (Ozkula and Uang, 2015). For a typical test, the target axial load was first applied to the specimen and held constant. Then the pseudo-static cyclic drift, computed as the AISC specified

Table 2. Steel Tensile Coupon Test Results				
Shape	Component	Yield Stress (ksi)	Tensile Strength (ksi)	Elongation* (%)
W24×176	Flange Web	52.5 58.5	81.8 82.5	38.1 38.0
W24×131	Flange Web	50.8 55.4	75.9 77.7	38.4 35.4
W24×104	Flange Web	51.5 58.1	78.0 80.6	36.5 31.3
W24×84	Flange Web	51.3 58.8	77.6 80.2	36.2 31.0
W24×55	Flange Web	53.7 59.8	71.5 74.3	38.0 32.4
* Based on a 2-in. gage length.				

story-drift angle multiplied by the column length (=18 ft), was applied to the moving end of the specimen.

DATA REDUCTION

In the following presentation, the story-drift ratio (SDR) is defined as the imposed lateral displacement, Δ, divided by the column length, L. Assuming an inflection point at the mid-height of the column, the end moment including the P-Δ effect is computed as

$$M = \frac{1}{2}(VL + P\Delta) \tag{4}$$

where V is the measured lateral load (i.e., column shear) and P is the measured axial load. End moment can be normalized by either the plastic moment, M_p, or the reduced plastic moment, M_{pc}. Reduced moment can be computed using Equation 5(a) for strong-axis and Equation 5(b) for weak-axis bending.

$$M_{pc} = 1.18\left(1 - \frac{P}{P_y}\right)M_p \le M_p \tag{5a}$$

$$M_{pc} = 1.19\left[1 - \left(\frac{P}{P_y}\right)^2\right]M_p \le M_p \tag{5b}$$

The measured yield stresses were used to compute these strengths.

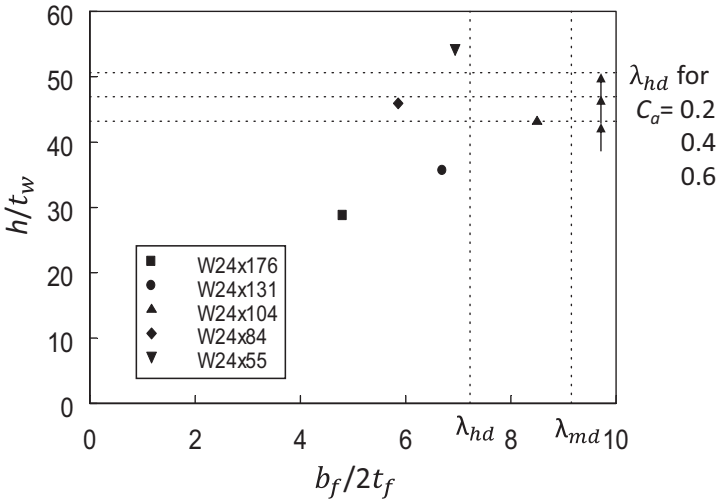

Fig. 1. Comparison of width-to-thickness ratios.

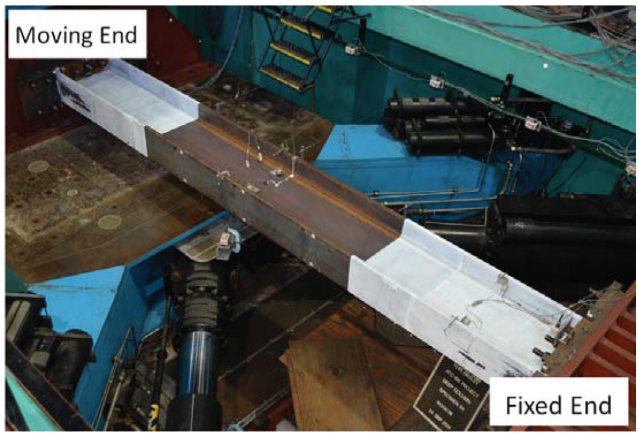

Fig. 2. Test setup.

EXPERIMENTAL RESULTS

Group 2: W24×131 Specimens

The flanges and webs of group 2 specimens are classified as highly ductile. This group with five specimens (2Z, 2L, 2LP, 2M, 2H) served as the reference group for comparison with the response of the other groups. To evaluate the effect of axial load, 2Z without an axial load was included in this group. This "beam" specimen was able to reach 7% drift without any strength degradation before one flange fractured near the weld access hole. Local buckling of the flanges and web in the plastic hinges was minimal. By increasing the level of axial force for the remaining specimens, local buckling of the flanges and web in the plastic hinges at the member ends became more significant. The lateral load versus story-drift ratio (SDR) responses in Figure 3 show that increasing the axial force level reduced the plastic moment, triggered local buckling at a lower drift, accelerated strength degradation in the post-yield region, and reduced the energy dissipation and deformation capacities. For example, local buckling was visible during 3% drift cycles for specimen 2L (C_a = 0.2), but local buckling was visible for specimen 2H (C_a = 0.6) at 0.75% drift cycles. Other than experiencing local buckling at both ends, the specimens showed no sign of global buckling (either FB or LTB).

Specimen 2L was cyclically tested up to 4% drift only. To evaluate the axial capacity of a flexurally yielded column, after unloading the lateral load, the specimen was then axially compressed in its residual position to axial failure. The specimen eventually experienced out-of-plane FB at 1500 kips. Assuming an effective length factor, K, of 1.0 and using a member length equal to the distance between the two plastic hinges (i.e., severely buckled regions, 187 in. = 0.86L), the expected compression strength per AISC 360 (AISC, 2010b) is 1465 kips, which correlates well with the

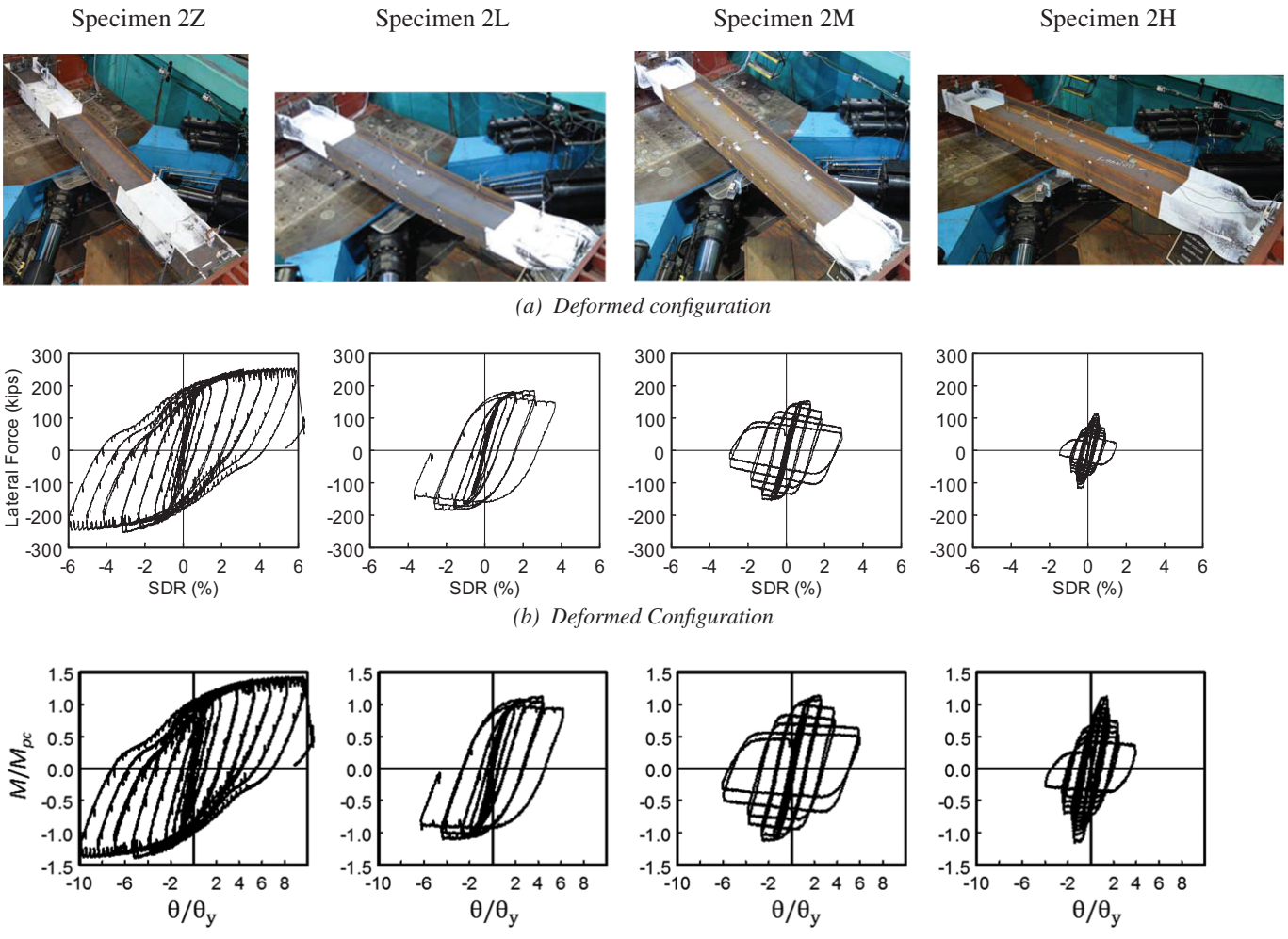

(a) Deformed configuration

(b) Deformed Configuration

(c) Normalized end moment vs. normalized story drift

Fig. 3. Group 2 (W24×131 section): Failure mode and hysteresis response.

measured value. To evaluate the cyclic loading effect, one extra specimen, 2L-P, was monotonically loaded to 4% drift, and this "pushover" response is compared with the backbone curve for specimen 2L in Figure 12(b).

Group 1: W24×176 Specimens

The flange and web of group 1 specimens are more compact than group 2 specimens. It was expected that more ductility could be developed from these specimens and the extent of local buckling would be less. However, testing showed that, unexpectedly, LTB was the dominant failure mode.

It was shown that specimen 2L started to show local buckling at 3% drift. The stockier section of specimen 1L delayed local buckling to 4% drift (see Figure 4). Note that the yielded length of this group of specimens was longer when compared with those of the other groups. By having a more compact section, the onset of local buckling was delayed, and it allowed more strain hardening to occur; see Table 3 for the cyclic strain hardening ratios (M_{max}/M_{pc}). The larger moment developed at the column ends resulted in a longer yielded length, wherein the Young's modulus was reduced drastically (see Figure 5). Therefore, the compressive flanges of the column were more prone to LTB. This illustrates the effect of cross-section compactness on the plastic hinge length, which in turn can influence the buckling mode.

By doubling the axial load for specimen 1M, local buckling started earlier, at 2% drift; the local buckling pattern at both ends of the column was antisymmetric. Long yielded zones at the column ends triggered the same LTB mode like specimen 1L. Tripling the axial load for specimen 1H produced local buckling at 1% drift, and the local buckling pattern at both ends of the column was symmetric. Long yielded lengths also triggered LTB, but high axial load together with the symmetric local buckling pattern caused the column to experience FB.

In summary, all three specimens first showed local buckling but eventually failed in global buckling. The yielded lengths were the longest among all groups tested due to the stockier cross-section. Specimen 1H showed

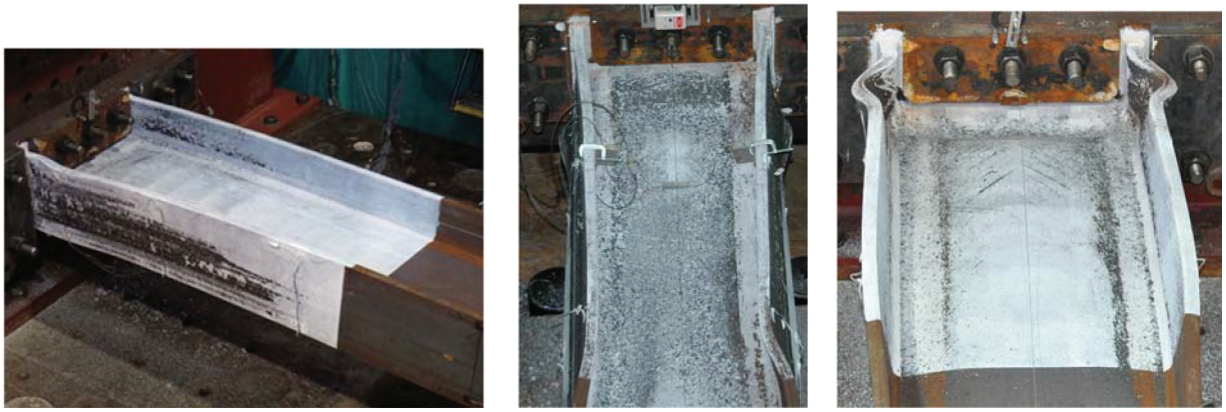

(a) Yielding and buckling pattern *(b) West end* *(c) East end*

Fig. 4. Specimen 1L: Deformation at column ends (7% drift).

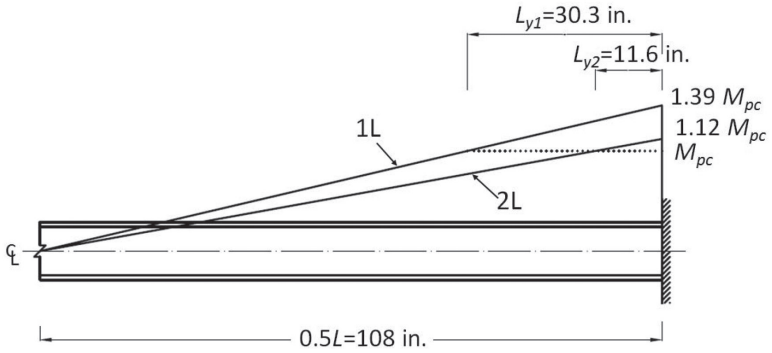

Fig. 5. Comparison of yielded length.

single-curvature FB, probably because the local buckling patterns at both ends were symmetric. Specimens 1L and 1M had antisymmetric local buckling patterns, and both failed in an S-shaped (double-curvature) LTB mode. Figure 6 shows the failure mode and hysteresis response of all three specimens.

Group 3: W24×104 Specimens

The webs of group 3 specimens are classified as highly ductile, and the flanges are classified as moderately ductile. All three specimens in this group experienced FLB first, which then interacted with WLB. Significant local buckling occurred at high drift levels or when the axial load was high, which was accompanied by considerable column shortening. No global buckling was observed. Depending on the direction of local buckling at member ends, one end at the buckled region might move out-of-plane in one direction, while the other end moved in either the same or opposite direction, thus causing the column segment in between to twist slightly as a rigid body. However, this deformation was not the result of global buckling. Figure 7 shows the failure mode and hysteresis response of all three specimens.

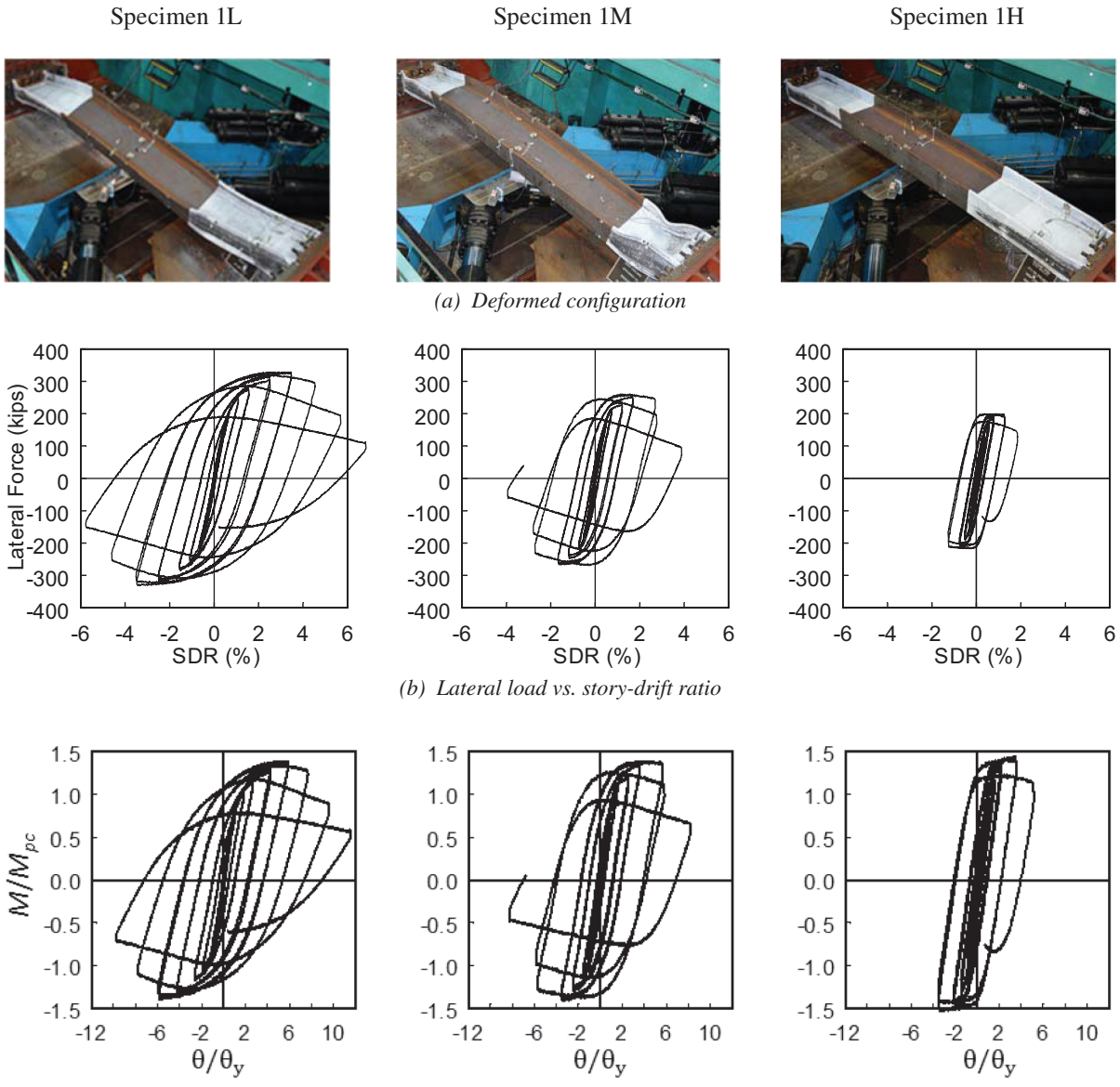

(a) Deformed configuration

(b) Lateral load vs. story-drift ratio

(c) Normalized end moment vs. normalized story drift.

Fig. 6. Group 1 (W24×176 section): Failure mode and hysteresis response.

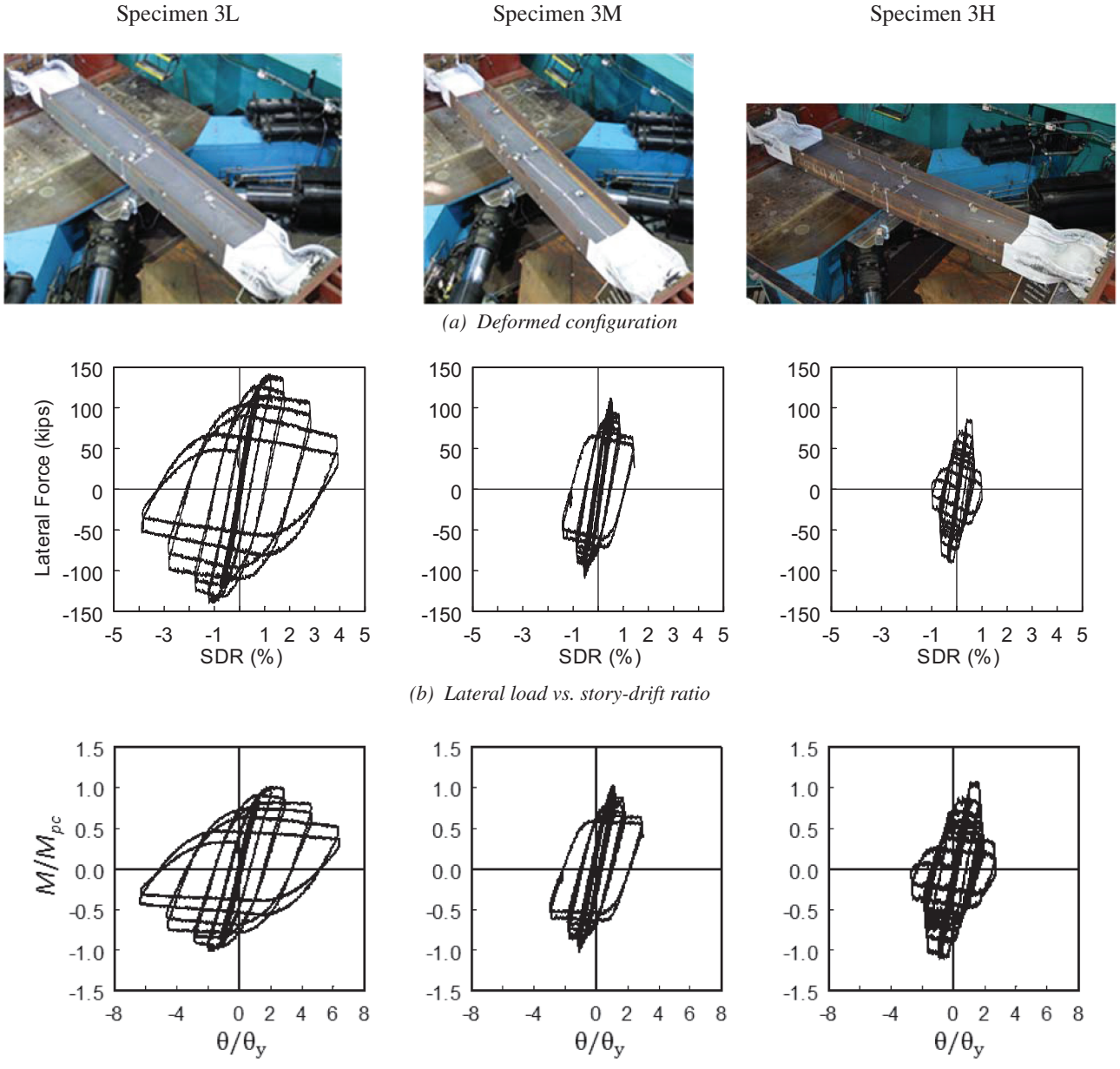

(a) Deformed configuration

(b) Lateral load vs. story-drift ratio

(c) Normalized end moment vs. normalized story drift.

Fig. 7. Group 3 (W24×104 section): Failure mode and hysteresis response.

Group 4: W24×84 Specimens

The flanges of group 4 specimens are classified as highly ductile, and the webs are classified as highly ductile for low axial load, but otherwise moderately ductile. Specimen 4L (C_a = 0.2) experienced brittle fracture near the weld access hole at 2% drift. It was decided not to test the specimen originally planned for high axial load (4H) so that testing of 4L could be repeated. Although the slenderness ratio for LTB of this group of specimens was about 50% higher than those of the first three groups, the specimens did not fail in LTB or FB. Instead, local buckling dominated the responses. Compared to groups 1 and 2 specimens, the larger width-to-thickness ratios of the webs caused the specimens to buckle along the entire depth of the webs, which in turn triggered local buckling of both flanges at each end. The direction of local buckling at one end of the column was reversed from that at the other end. Therefore, both specimens failed in a double-curvature configuration. Because local buckling developed along the full section depth, axial shortening was significant. Figure 8 shows the failure mode and hysteresis response for both specimens.

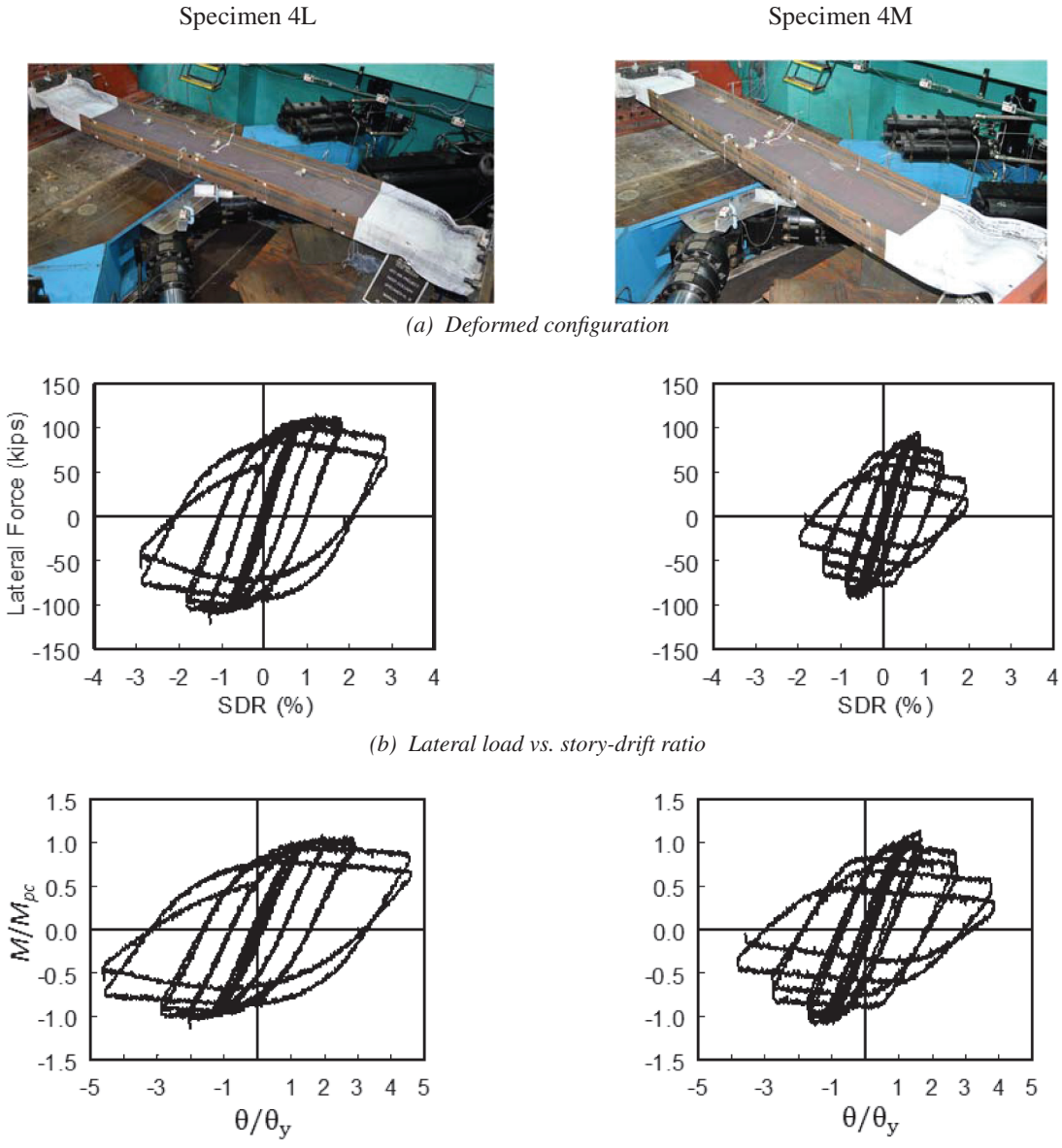

(a) Deformed configuration

(b) Lateral load vs. story-drift ratio

(c) Normalized end moment vs. normalized story drift.

Fig. 8. Group 4 (W24×84 section): Failure mode and hysteresis response

Group 5: W24×55 Specimens

Three specimens were planned for this group. After testing 5L (C_a = 0.2) and 5M (C_a = 0.4), it was observed that the measured ductility capacity was small. Instead of testing the last specimen (5H) at the high axial load (C_a = 0.6), it was decided to test it with an intermediate C_a value of 0.3; the specimen was designated as 5LM. The slenderness ratio for LTB was 2.2 times that of the group 2 specimens. The flanges are classified as highly ductile, and the webs did not meet the highly ductile requirement; specimen 5L was below, 5LM was practically at and 5M exceeded the limiting value for a moderately ductile web.

With little sign of local buckling, specimen 5L experienced LTB during the 1.5% drift cycles. Alternating loading caused the same (south) flange to buckle in the same (upward) direction. The deformation amplitude was significant at 2% drift before the test was stopped. Figure 9(a) shows that LTB caused the middle portion of the column to tilt about its longitudinal axis. Local buckling was observed at one end, but it was triggered by LTB. Specimens 5LM

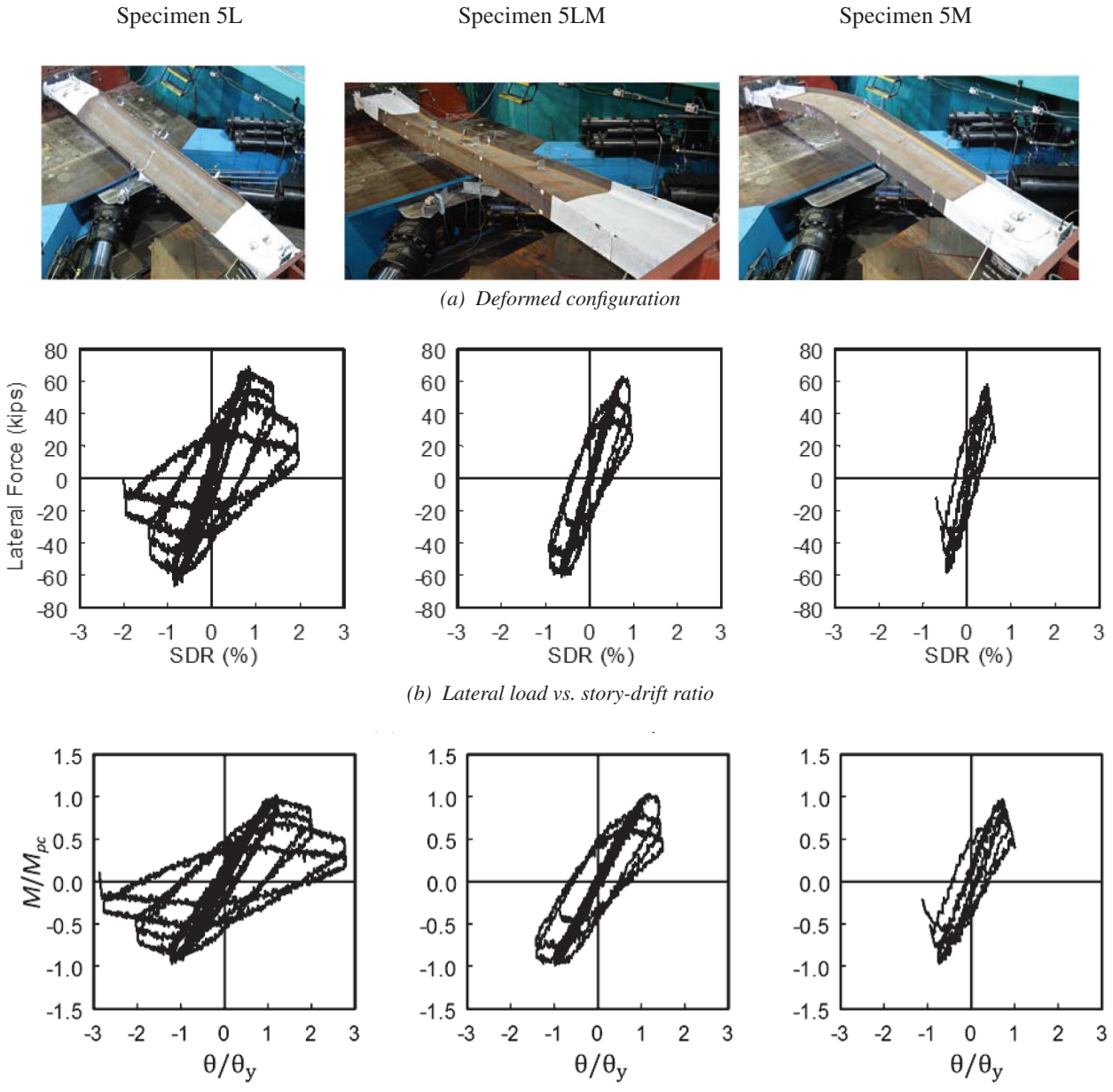

(a) Deformed configuration

(b) Lateral load vs. story-drift ratio

(c) Normalized end moment vs. normalized story drift.

Fig. 9. Group 5 (W24×55 section): Failure mode and hysteresis response.

and 5M also showed LTB first at lower drift levels. But specimen 5M turned to FB about the weak axis during the fourth negative excursion to 0.75% drift. Specimen 5LM also turned to the same FB mode but at a slightly higher (1%) drift level. The failure mode and hysteresis response are shown in Figure 9.

Group 6: W24×131 Specimens

Specimens from groups 6 and 2 had the same shape and material properties, except that the former specimens were subjected to weak-axis bending. Specimen 6L was tested up to 7% drift. As expected, LTB was not a concern for weak-axis bending. But local buckling observed in the nominally identical specimen 2L did not occur in specimen 6L, and the specimen performed in a ductile manner. Because the AISC *Specification* compactness requirement for wide-flange sections does not distinguish between strong- and weak-axis bending, testing of specimen 6L clears shows that the AISC *Specification* compactness criterion for weak-axis bending is very conservative. Upon unloading the lateral load, it was decided to monotonically compress the column in order to evaluate the residual axial load capacity. The specimen failed by weak-axis flexural buckling at an axial load of 1627 kips. After observing the stable response of

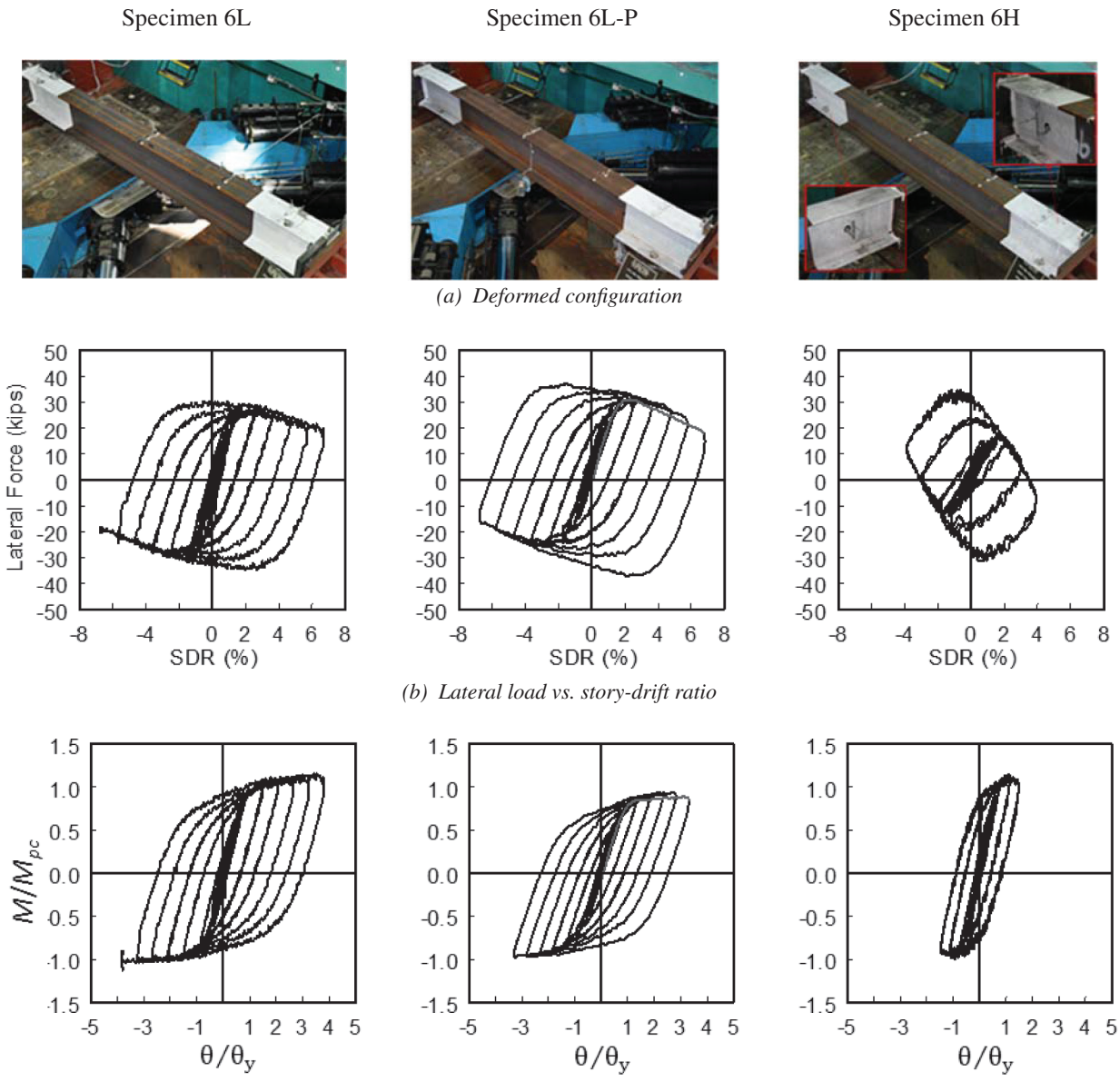

(a) Deformed configuration

(b) Lateral load vs. story-drift ratio

(c) Normalized end moment vs. normalized story drift.

Fig. 10. Group 6 (W24×131 section): Failure mode and hysteresis response.

Table 3. Member Overstrength and Rotational Capacity					
Specimen	M_{max} (kip-ft)	M_{max}/M_{pc}	θ_{yc} (×0.01 rad)	θ_p (×0.01 rad)	R_p
1L	3148	1.39	0.61	3.99	6.54
1M	2423	1.38	0.50	2.42	4.84
1H	2010	1.43	0.38	1.15	3.03
2Z	2327	1.41	0.63	4.95	7.98
2L	1655	1.12	0.60	2.91	4.85
2M	1430	1.13	0.49	1.07	2.18
2H	1084	1.10	0.37	0.28	0.76
3L	1262	1.03	0.62	2.82	4.55
3M	880	0.99	0.50	0.96	1.92
3H	779	1.03	0.38	0.68	1.79
4L	1039	1.05	0.63	2.85	4.52
4M	897	1.12	0.51	1.32	2.59
5L	599	1.02	0.69	0.60	0.87
5LM	594	1.03	0.63	0.26	0.41
5M	494	1.00	0.61	N.A.	N.A.
6L	454	1.15	1.78	5.68	3.19
6L-P	406	0.93	1.79	5.61	3.13
6H	337	1.14	1.74	3.49	2.00

specimen 6L, it was decided to triple the axial load and test specimen 6H. Under high axial load, minor web and flange buckling at both ends developed. The test was stopped at 4% drift due to the significant *P*-Δ effect; the lateral resistance practically diminished at this drift level.

To evaluate the cyclic loading effect, it was then decided to laterally load the third specimen (6L-P) to 7% drift in order to generate a monotonic response for comparison with the backbone curve of specimen 6L. Thereafter, the specimen was subjected to the AISC loading protocol in a reverse sequence from 7% drift to evaluate the loading sequence effect. As shown in Figure 10, the sequence of loading did not affect the failure mode nor the strength of the column. But the post-buckling negative stiffness was reduced somewhat when the AISC loading protocol was applied in a reverse sequence.

ANALYSIS OF TEST RESULTS

Backbone Curves and Member Overstrength

The backbone curve of each cyclically loaded specimen was derived from the first cycle of each story-drift level (ASCE, 2013) as shown in Figure 11(a). The backbone curves of each of the six groups in Figure 12 show that the level of axial load significantly affected both the strength and plastic rotation capacity of the columns.

It was observed from the behavior of group 1 specimens that significant strain hardening could alter the failure mode and trigger global buckling mode. The cyclic strain hardening ratio is evaluated as the ratio between the maximum end moment and the reduced plastic moment, M_{pc}, in Equation (5a). The ratios thus computed are listed in Table 3.

Plastic Rotation Capacity

The plastic rotation, θ_p, can be evaluated from the backbone curve by the procedure shown in Figure 11(b). The plastic rotation capacity, R_p, is then computed as

$$R_p = \frac{\theta_T - \theta_y}{\theta_y} = \frac{\theta_p}{\theta_y} \tag{8}$$

Figure 13(a) shows the effect of axial force level on the plastic rotation of six groups of specimens. The weak-axis specimens (group 6) delivered the highest plastic rotations. Under strong-axis bending, the slenderness ratios for both local and global buckling in addition to axial force level had a significant effect on the plastic rotation capacity. Assuming that a beam-to-column connection in an SMF is expected to achieve a story-drift angle of 0.04 radian, taking the elastic

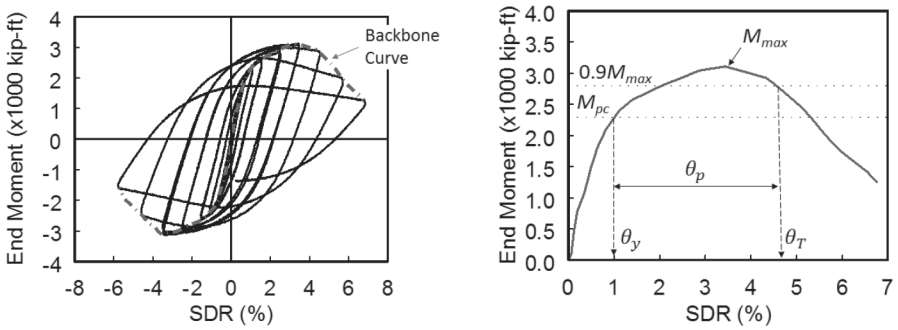

(a) Backbone curve *(b) Rotation capacity*

Fig. 11. Definition of backbone curve and rotation capacity.

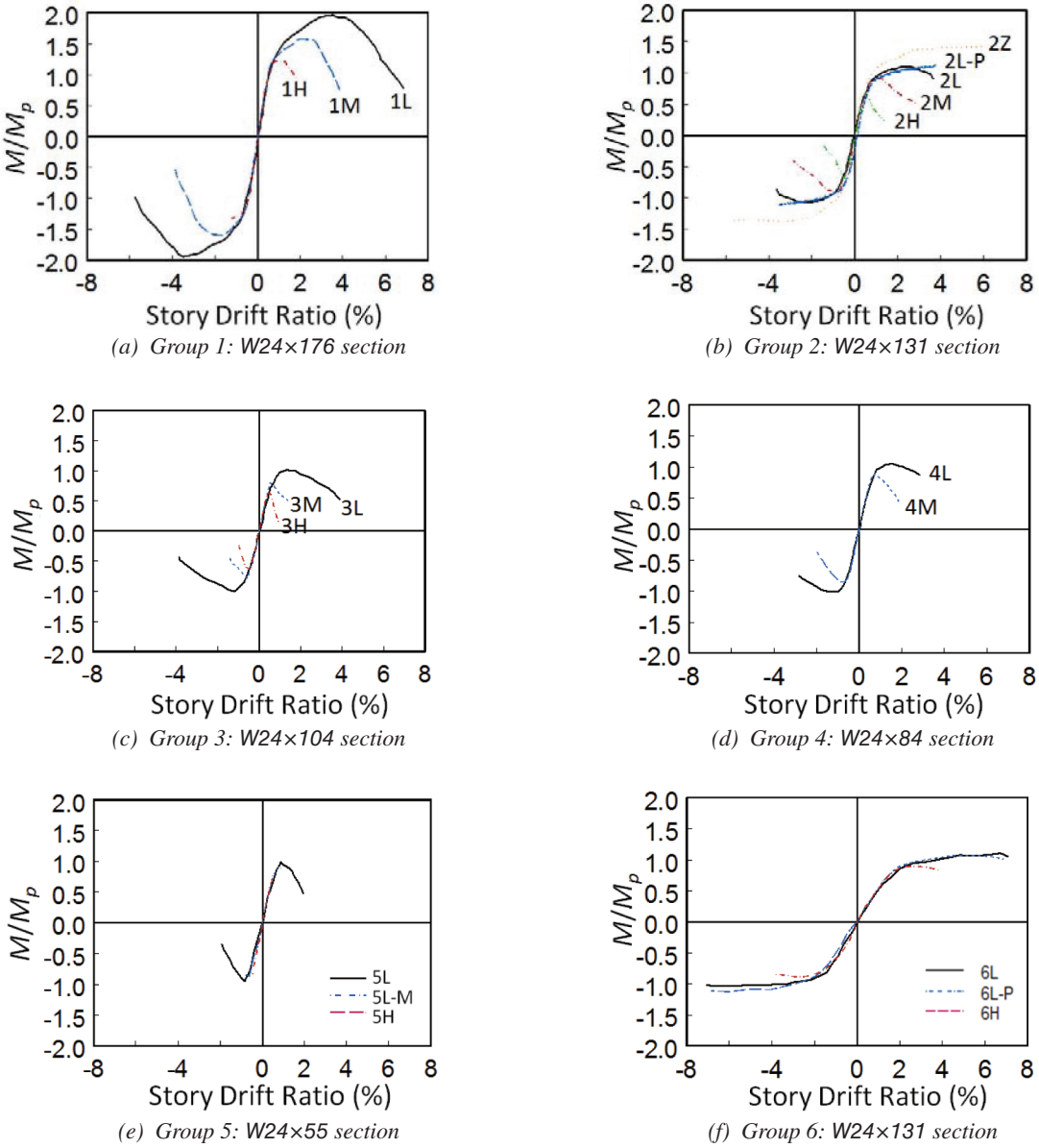

(a) Group 1: W24×176 section *(b) Group 2: W24×131 section*

(c) Group 3: W24×104 section *(d) Group 4: W24×84 section*

(e) Group 5: W24×55 section *(f) Group 6: W24×131 section*

Fig. 12. Comparison of backbone curves.

component as 0.01 radian, the plastic rotation demand would be 0.03 radian. Figure 13(a) shows that the majority of deep column specimens failed to deliver this rotation.

The plastic rotation capacities of the deep, slender W24 columns tested in this research program can be compared with those of the stockier W14 columns tested by Newell and Uang (2008); these W14 columns had a $b_f/2t_f$ ratio up to 7.2 and a h/t_w ratio up to 17.7. Taking a W14×233 column specimen ($b_f/2t_f$ = 4.62 and h/t_w = 10.7) under cyclic axial loading with a peak C_a value of 0.6 for example, local buckling was limited even for a drift up to 0.08 rad. In-plane plastic hinging developed at both ends of the column, and the plastic rotation capacity reached 15, much higher than those of the W24 columns tested in this test program.

Axial Shortening

With the presence of a constant axial force, most of the column specimens showed significant shortening after severe local buckling or global buckling occurred. The measured shortenings are summarized in Figure 14. Two plots are presented for each group. The first plot compares the shortenings at the end of each test. To show the effect of axial force level, the second plot compares shortenings at a given drift level; the effect of axial force level is obvious from these plots. Note that most of the nonlinear analysis software for performance-based seismic evaluation cannot model column shortening due to buckling. This effect on the margin against collapse at the system level remains to be investigated.

CONCLUSIONS

Based on the test results of 21 W24 column specimens subjected to cyclic loading with varying levels of constant axial load, the following observations can be made:

1. The slenderness ratios for local buckling and LTB had a significant effect on the failure mode (local versus global buckling).
2. The level of axial load affected the plastic rotation capacity. Most of the strong-axis bending specimens were not able to deliver a plastic rotation of 0.03 radian (see Figure 13).
3. The presence of an axial load produced significant local buckling and axial shortening (see Figure 14).
4. Having a seismically very compact section with low width-to-thickness ratios may trigger LTB after local buckling occurs (see Figure 6 for the failure mode of group 1 specimens). The switch from local buckling to LTB was due to significant strain hardening, which extended the yielded length. From the viewpoint of post-earthquake, gravity load-carrying capacity, having a column experiencing in-plane plastic hinging with local buckling is more desirable than that experiencing global buckling of the member.
5. Specimens with weak-axis bending were ductile, showing little local buckling up to a very high drift level (see Figure 10). The AISC compactness requirement for W-shaped members with weak-axis bending is very conservative.

Because the number of tests conducted in this study was limited, more tests including those with different column depths have been planned to enhance the statistical significance of the test database. Together with supplementary analytical studies, design recommendations on the appropriate limiting cross-section element and member slenderness ratios for seismic design and assessment of steel moment frames will be provided at a later time.

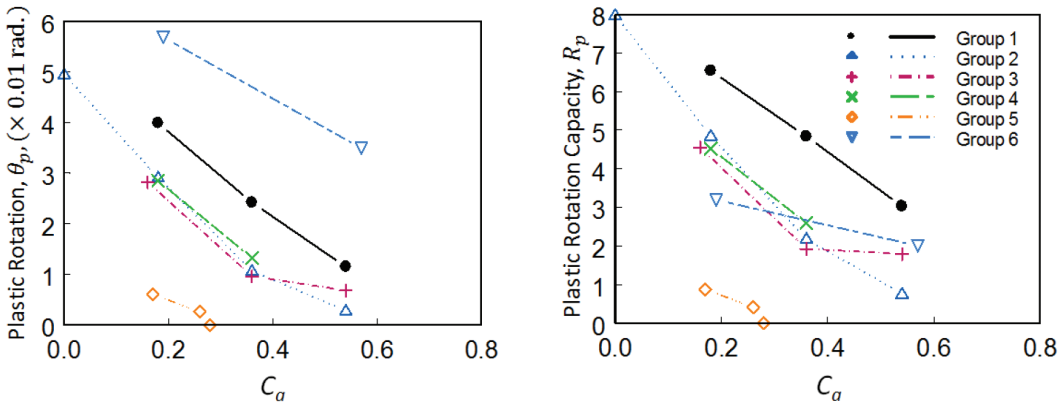

(a) Plastic rotation vs. C_a *(b) Plastic rotation capacity vs. C_a*

Fig. 13. Plastic rotation and plastic rotation capacity.

ACKNOWLEDGMENTS

Funding for this research was provided by the NEHRP Consultants Joint Venture under its Earthquake and Structural Engineering Research contract with the National Institute of Standards and Technology. J.O. Malley from Degenkolb Engineers chaired the Project Advisory Committee, and A. Hortacsu from the Applied Technology Council served as the Project Manager. The authors also would like to acknowledge the American Institute of Steel Construction for providing steel materials and The Herrick Corporation for fabricating the test specimens.

DISCLAIMER

NIST policy is to use the International System of Units (metric units) in all its publications. In this paper, however, information is presented in U.S. Customary Units (inch-pound) because this is the preferred system of units in the U.S. earthquake engineering industry.

REFERENCES

AISC (2010a), *Seismic Provisions for Structural Steel Buildings*, ANSI/AISC 341-10, American Institute of Steel Construction, Chicago, IL.

AISC (2010b), *Specification for Structural Steel Buildings*, ANSI/AISC 360-10, American Institute of Steel Construction, Chicago, IL.

(a) Group 1 (W24×176 section)

(b) Group 2 (W24×131 section)

(c) Group 3 (W24×104 section)

Fig. 14. Column axial shortening.

ASCE (2013), *Seismic Evaluation and Retrofit of Existing Building Structures*, ASCE/SEI 41-13, American Society of Civil Engineers, Reston, VA.

ASTM (2012), *Standard Specification for Structural Steel Shapes,* A992/A992M-11, American Society for Testing and Materials, Vol. 01.04, West Conshohocken, PA.

Newell, J.D. and Uang, C.-M. (2008), "Cyclic Behavior of Steel Wide-Flange Columns Subjected to Large Drift," *Journal of Structural Engineering*, ASCE, Vol. 134, No. 8, pp. 1334–1342.

NIST (2011), *Research Plan for the Study of Seismic Behavior and Design of Deep, Slender, Wide-Flange Structural Steel-Beam-Column Members*, NIST-GCR-11-917-13. Produced by the NEHRP Consultants Joint Venture, a partnership of the Applied Technology Council and the Consortium of Universities for Research in Earthquake Engineering, for the National Institute of Standards and Technology, Gaithersburg, MD.

Ozkula, G. and Uang, C.-M. (2015), "Seismic Behavior and Design of Deep, Slender Wide-Flange Structural Steel Beam-Column Members," Report No. SSRP-15/06, Department of Structural Engineering, University of California, San Diego, La Jolla, CA.

(d) Group 4 (W24×84 section)

(e) Group 5 (W24×55 section)

Fig. 14. Column axial shortening (continued).

DISCUSSION

Observations from Cyclic Tests on Deep, Wide-Flange Beam-Columns

Paper by GULEN OZKULA, JOHN HARRIS and CHIA-MING UANG
(First Quarter 2017)

Discussion by BRUCE F. MAISON

The writer congratulates the authors for a truly impressive number of lab tests on beam-columns (Ozkula et al., 2017). Such data are valuable for advancing our knowledge of actual component behaviors in step with the gaining popularity of performance-based seismic design. The purpose of this Discussion is to point out that component backbone curves are strongly influenced by the specimen loading history (protocol) used in lab tests, and realistic seismic loading protocols ought to be included when formulating backbone curves.

The loading protocols used in the authors' tests were mostly those from AISC 341 (AISC, 2010) consisting of fully reversed cyclic loading at progressively increasing peak displacement amplitudes. The AISC 341 loading protocol is for moment connection qualification in new construction. It provides evidence that a component satisfies certain ductility requirements and is a consistent way to compare the relative performance of different components. The protocol does not mimic actual earthquake loading histories and is *not* specifically intended for use in backbone curve formulation. As a result, backbone curves derived from the envelope of cyclic test data may not adequately describe component behavior at near-collapse inelastic displacement levels (FEMA, 2009). The component ductility can be significantly underestimated. Loading protocols used in tests to demonstrate connection qualification are not the same as those for backbone curve formulation.

Figure 1 illustrates the significant difference in component response resulting from the loading protocol used in the test. A backbone curve based on the cyclic envelope would be appropriate if the earthquake generates numerous fully reversed cycles of response, but the monotonic test would be a better backbone if the quake generates few cycles. Near-collapse seismic response is more like a monotonic as opposed to fully reversed cyclic loading (Krawinkler, 2009). Note how the strength deterioration in the authors' backbone curve is an artifact from the load reversal points in the loading protocol.

The authors' study included one test of strong-axis bending under monotonic loading. Backbone curves for the Group 2 tests (W24×131) are shown in Figure 2. Specimen 2L-P (monotonic loading) had no strength deterioration at a story-drift ratio (SDR) of 4%. However, specimen 2L (fully reversed cyclic loading) had notable strength deterioration. The authors' observation that most of the strong-axis bending specimens were not able to deliver a plastic rotation of 0.03 radian is relevant to AISC 341 component qualification requirements. However, in the context of actual earthquake performance, the observation is not as ominous as might be perceived by the casual reader. Albeit, more tests using realistic earthquake loading histories are needed for confirmation.

The new ASCE 41-17 (2017) recognizes the importance of loading protocols and provides additional freedom in protocol selection to better reflect actual seismic demand patterns. It does not prescribe a specific "one-size-fits-all" loading protocol due to the wide variation of factors involved with a particular component—for example, performance objective, type of structure, and seismic setting. To ensure reasonable protocols are selected for a particular component and project, concurrence is required by independent peer reviewers experienced with the use of test data in design and analysis of structures.

Figure 3 shows a loading protocol depicting a median building response from a maximum considered earthquake (MCE). It is based on statistics from analysis of a four-story building model subjected to numerous earthquake records (Maison and Speicher, 2016). Note how the protocol has a bias in the positive direction and relatively few response cycles. A monotonic push to component failure is added at the end of the cycling portion to capture response at large near-collapse displacement levels. Another protocol based on long duration earthquakes has a similar pattern but with more response cycles (Maison and Speicher, 2018).

Because most prior component tests were performed using fully reversed cyclic loadings, ASCE 41-17 allows

Bruce F. Maison, Consulting Engineer, El Cerrito, CA.
Email: maison@netscape.com

Paper No. 2015-16DR

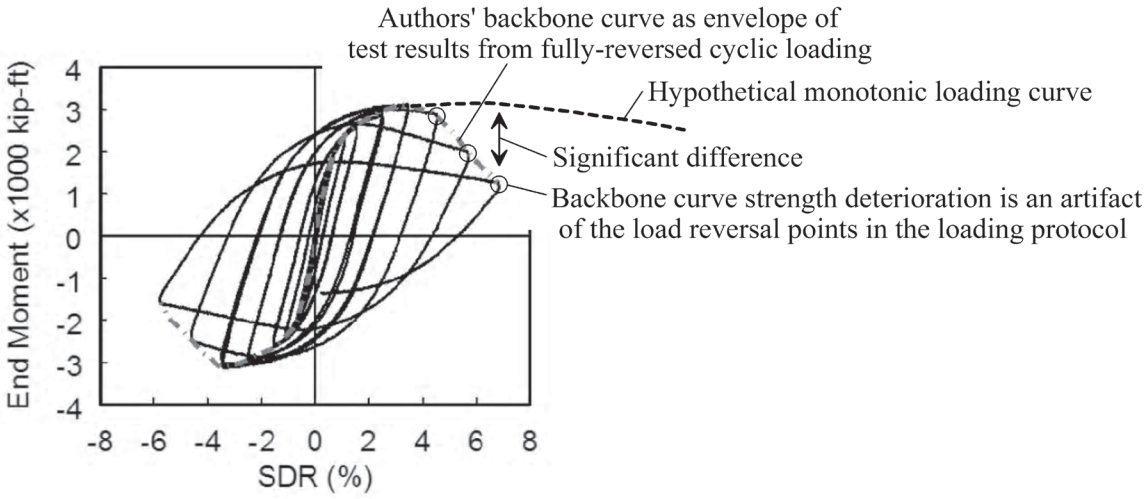

Fig. 1. Comparison of backbone curves derived from fully reversed and monotonic loading protocols (adapted from Fig. 11a of Ozkula et al., 2017).

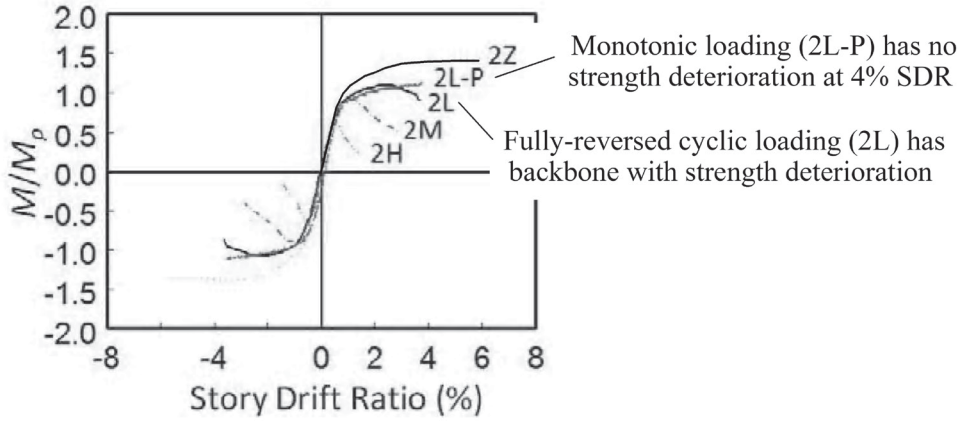

Fig. 2. Backbone curves derived from Group 2 (W24×131) lab tests (adapted from Fig. 12b of Ozkula et al., 2017)

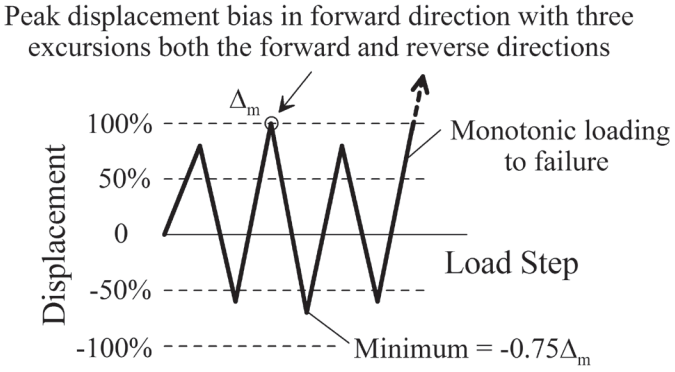

Fig. 3. MCE level median loading protocol (adapted from Fig. 18 of Maison and Speicher, 2016).

such test data to be supplemented to better define behavior at large near-collapse displacement levels. It is permitted to combine cyclic and monotonic test data in the formulation of backbone curves in cases where the cyclic tests show specimen strength degradation that is an artifact of the loading protocol as that shown in Figure 1. Figure 4 from ASCE 41-17 illustrates one way this can be done. As a precaution, a displacement limit is placed in the monotonic data leading to the abrupt decline in the backbone at point *E*.

In closing, the writer appreciates the value of the authors' research but encourages the inclusion of test data from realistic earthquake and/or monotonic load patterns in the future to supplement AISC 341 cyclic testing, thus providing more comprehensive results that are better suited for ASCE 41 backbone curve formulation.

REFERENCES

AISC (2010), *Seismic Provisions for Structural Steel Buildings,* ANSI/AISC 341-10, American Institute of Steel Construction, Chicago, IL.

ASCE (2017), *Seismic Rehabilitation of Existing Buildings*, ASCE/SEI 41-17, American Society of Civil Engineers, Reston, VA.

FEMA (2009), "The Effects of Strength and Stiffness Degradation on Seismic Response," Technical Report FEMA P-440A, Federal Emergency Management Agency, Washington, DC.

Krawinkler, H. (2009), "Loading Histories for Cyclic Tests in Support of Performance Assessment of Structural Components, *Proceedings of the 3rd International Conference on Advances in Experimental Structural Engineering (3AESE)*, San Francisco, October.

Maison, B.F., and Speicher, M.S. (2016), "Loading Protocols for ASCE 41 Backbone Curves," *Earthquake Spectra*, Vol. 32, No. 4, November.

Maison, B.F., and Speicher M.S. (2018), "Importance of Experiment Loading Protocols in Developing ASCE 41-17 Backbone Curves," *11th U.S. National Conference on Earthquake Engineering,* Earthquake Engineering Research Institute, Los Angeles, CA, June.

Ozkula, G., Harris, J., and Uang, C.M. (2017), "Observations from Cyclic Tests on Deep, Wide-Flange Beam-Columns," *Engineering Journal*, AISC, Vol. 54, No. 1, pp. 45–59.

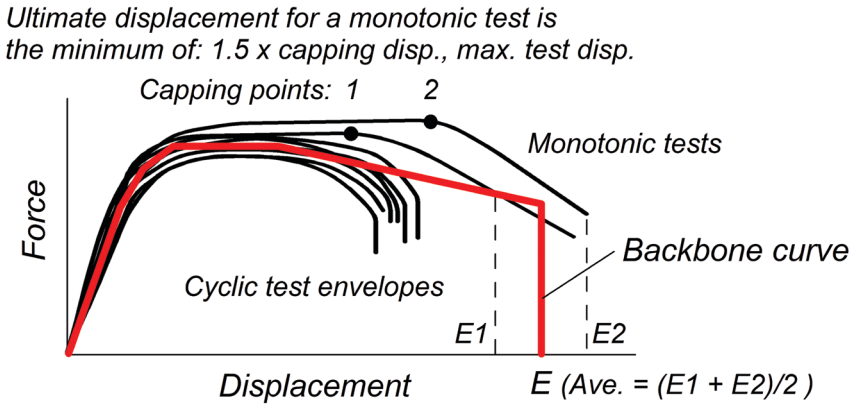

(b) Backbone curve construction using cyclic test envelopes supplemented with monotonic tests

Fig. 4. Illustration of backbone curve derived from combination of cyclic and monotonic test data [adapted from Fig. 7-6 of ASCE 41-17 (2017)].